



# CONTRASTING SUBSURFACE MODELS FOR PHYSICS-BASED REGIONAL-SCALE NUMERICAL SIMULATIONS IN JAPAN USING A RIGOROUS VALIDATION SCHEME

Swasti SAXENA<sup>1</sup>, Ramin MOTAMED<sup>2</sup> and Keri RYAN<sup>3</sup>

<sup>1</sup> Postdoctoral Research Associate, Environmental Subsurface Science Group, Pacific Northwest National Lab, Seattle, WA, USA, swasti.saxena@pnnl.gov

<sup>2</sup> Associate Professor, Department of Civil and Environmental Engineering, University of Nevada, Reno, NV, USA, motamed@unr.edu

<sup>3</sup> Professor, Department of Civil and Environmental Engineering, University of Nevada, Reno, NV, USA, klryan@unr.edu

**ABSTRACT:** At regional scales, modeling the subsurface structure for physics-based numerical simulations poses a challenge, hence two of the most common modeling techniques are juxtaposed in this study. Simulations from both models are carried out using a seismic modeling code SW4 for two aftershocks of the 2007 Niigata Chuetsu-Oki earthquake and validated against recorded data from Kashiwazaki-Kariwa Nuclear Power Plant and three K-NET stations in the form of waveforms, response spectra, amplification factors and goodness-of-fit, which highlight the importance of geotechnical layers in capturing the site-specific response. Regional attenuation of ground motions from the two subsurface models is compared with recorded peak ground accelerations in the region and NGA-West2 ground motion prediction equations, revealing the realistic scattering pattern that can only be replicated by acknowledging a 3D subsurface structure. In conclusion, both the models have their individual merits and limitations that are reported after extensive qualitative and quantitative validations.

**Keywords:** *Regional-scale physics-based simulations, 2007 Niigata-Chuetsu aftershocks, Community velocity models, Sedimentary layering, NGA-West2 GMPEs*

## 1. INTRODUCTION

Ground motion simulations carried out in the past decades (Boore<sup>1</sup>) and Hartzell<sup>2</sup>) have given birth to several methodologies to address their efficiency and accuracy, for example, finite-difference methods (Boore<sup>1</sup>, Olsen et al.<sup>3</sup>, Graves<sup>4</sup>, Pitarka<sup>5</sup>, Sjogreen and Petersson<sup>6</sup>), finite element methods (Bao et al.<sup>7</sup>, Gatti et al.<sup>8</sup>), and spectral methods (Peter et al.<sup>9</sup>, Afanasiev et al.<sup>10</sup>). Broadband simulations of seismic events are gaining significance to supplement missing data from earthquake catalogues and improve the ground motion models to reduce uncertainty by removing ergodic

assumptions (Anderson and Brune<sup>11</sup>). With the advent of high-performance computing, it is now possible to follow physics-based wave propagation from source to site in deterministic seismic simulation models (Rodgers et al.<sup>12</sup> and McCallen et al.<sup>13</sup>).

Latest advancements in deterministic numerical simulations are focused on pushing the computational resolution to higher frequencies for enhanced application in engineering (Gatti et al.<sup>8</sup>, McCallen et al.<sup>14</sup>). However, higher output frequencies require a smaller mesh size, which tend to be considerably small when the shear wave velocity ( $V_s$ ) at the surface is very low, in basins, for instance, and exponentially increase the demand on computational resources. To demonstrate, if the output frequency of a simulation is doubled, it would require the mesh size to be halved, leading to  $2 \times 2 \times 2$  times the number of grid points in three dimensions (3D), and double the processing time. Hence, to double the output frequency of a simulation, one would need  $2^4$  times or 16 times the computational resources. Given such limitations, the lowest shear wave velocity,  $V_{s_{min}}$ , attempted in regional simulations until this point has been 200 m/s (Taborda and Bielak<sup>15</sup>). Sedimentary basins with low  $V_{s_{min}}$  have a direct effect on the frequency content of simulated ground motions and surface amplifications, as concluded in Rodgers et al.<sup>12</sup>, and thus addressing  $V_{s_{min}}$  in the subsurface model of a basin is vital to the fidelity of the simulations.

Simulation of a seismic event is a function of its source, path, and site parameters. In regional-scale simulations, a popular method is to utilize well-constrained regional velocity models which characterize the deeper geology in 3D but often lack low-velocity information at the surface. This method is effective in modeling source-to-site path effects and scattering of seismic waves but may lead to inaccurate site amplifications if the model does not capture near surface velocities (as most models do not), especially in the basins. The second popular method employs horizontal sedimentary layers containing near surface geotechnical properties from a 1D soil profile but lacks subsurface heterogeneity in 3D. In this study, both of these techniques are contrasted under regional-scale simulations of two aftershocks of the 2007 Niigata-Chuetsu earthquake (NCEQ07) for their individual advantages and limitations. The numerical simulations are carried out using a fourth-order finite difference code developed by Lawrence Livermore National Laboratory known as SW4<sup>16</sup>, to solve viscoelastic wave propagation equations in space and time. SW4 is selected because of its advanced optimization techniques like mesh refinement, which permits variable mesh sizes for increasing shear wave velocities in a depth profile to save computational resources, and implementation of node-dependent message passing interface (MPI) which executes parallel processing on a massive scale thus exponentially reducing the computational time.

The site of interest in this research is Kashiwazaki-Kariwa Nuclear Power Plant (KKNPP) in Japan, which was the largest nuclear power plant in the world until it was shut down due to safety concerns when the NCEQ07 caused more than twice the design PGA at one of the reactors (Kayen et al.<sup>17</sup>). Tokyo Electric Power Company (TEPCO) has provided recorded ground motions for the NCEQ07 mainshock and six aftershocks at KKNPP at three free-field geotechnical arrays, two seismic observation sheds, and seven instrumented reactor and turbine buildings. The spatial variability of the subsurface soil at KKNPP has been reviewed in Pavlenko and Irikura<sup>18</sup> and Uetake et al.<sup>19</sup>, following which the authors also conducted a site characterization study (Saxena et al.<sup>20</sup>). From Taxonomy, horizontal-to-vertical spectral ratio (HVSr), and wavefield coherency, they ascertained the need for 3D modeling at KKNPP as a whole; however, one of the downhole arrays (Service Hall Array) displayed 1D site characteristics. The seismic events simulated in this study are small-to-moderate sized shallow crustal aftershocks of NCEQ07 to prevent any occurrence of soil nonlinearity in the layers with low shear wave velocities, and are generated using simple point-source models to remove any bias due to complex fault rupture models. The source parameters (moment magnitude- $M_w$ , seismic moment- $M_0$ , depth, strike, dip, and rake) obtained from F-net (Kubo et al.<sup>21</sup>) are presented in Table 1;  $M_{JMA}$  is the earthquake magnitude estimated by the Japan Meteorological Agency. Hereafter, aftershock 1,  $M_w$  3.5, will be referred to as Event 1 and aftershock 2,  $M_w$  4.4, as Event 2. Both events are simulated using the two subsurface models, which make a total of four simulations.

Table 1 Source parameters for simulated seismic events

Aftershock	$M_{JMA}$	$M_W$	$M_0$ (Nm)	Depth (km)	Strike; Dip; Rake [°]
07/16/2007 17:42 (Event 1)	4.2	3.5	$2.09 \times 10^{14}$	5	211; 54; 166
07/16/2007 21:08 (Event 2)	4.4	4.4	$5.21 \times 10^{15}$	11	39; 41; 115

Figure 1 shows the locations of KKNPP and nearby stations from the Kyoshin Network (K-NET) and Kiban Kyoshin network (KiK-net). The two seismic sources (corresponding to simulated events), KKNPP, and the three K-NET stations lay inside the computational boundary of the SW4 model (42.8 km x 41.9 km), highlighted by a pink box in the figure. All stations of importance, whether recorders or sources, are placed at least 30 grid points away from the computational boundary as per the recommendations of the SW4 User's Guide<sup>22</sup>. Two cross-sections, A-A' and B-B', are defined in the figure with KKNPP at their intersection to subsequently compare the 3D geomaterial model in the paper.

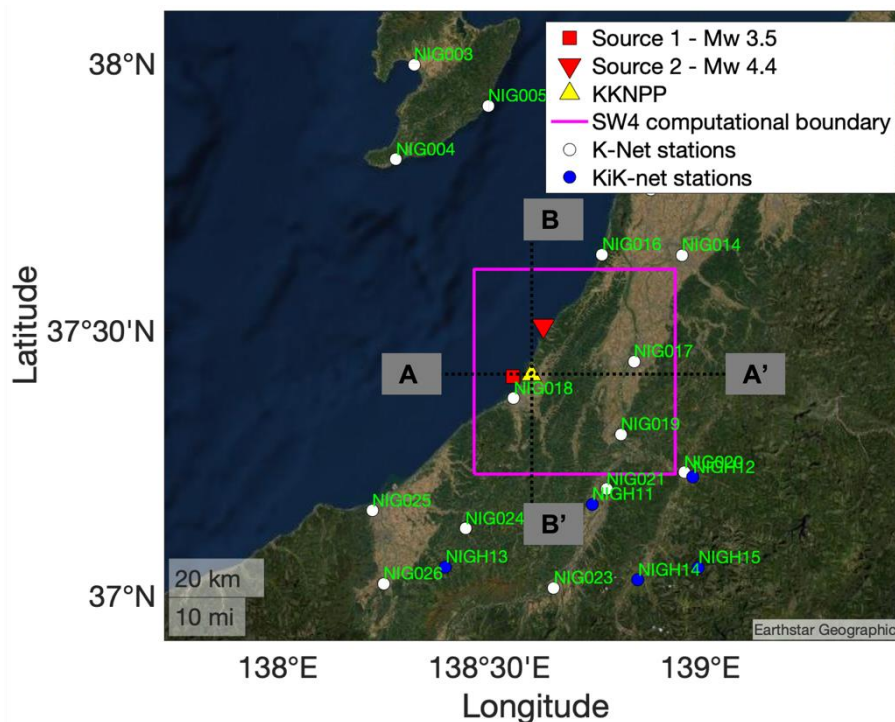


Fig. 1 Map of Japan showing KKNPP, K-NET and KiK-net stations in the region, and the location of the two seismic sources. Pink box denotes the computational boundary in SW4, and A-A' and B-B' are two cross-sections defined across the model.

Validation of different aspects of simulated ground motions is just as essential as the simulation of ground motions itself, a task undertaken by several researchers in the past. For example, the goodness-of-fit scheme proposed by Anderson<sup>23</sup> in 2004 has been differently adapted by Olsen and Mayhew<sup>24</sup>, Taborda and Bielak<sup>15</sup>, and Shi and Asimaki<sup>25</sup>, with distinctive modifications to validate simulations with recorded ground motions. While Rodgers et al.<sup>12), 26</sup> compared simulations with empirical ground motion models (GMMs), Lee et al.<sup>27</sup> used both methods to validate their simulations. On the other hand, Petrone et al.<sup>28</sup> devised a validation algorithm for non-historical earthquakes by carefully selecting a database of consistent real earthquakes. It is noteworthy that very few of these studies included vertical ground motions in their validation schemes. A unique feature of this study is a thorough performance assessment of horizontal and vertical ground motion simulations by employing a rigorous validation scheme including qualitative and quantitative

validation techniques at site-specific as well as regional levels, in a total of six validation exercises. For site-specific validation of Event 1 and Event 2, recorded ground motions are utilized from Service Hall Array (SHA), one of the free-field downhole arrays at KKNPP, and three K-NET stations inside the SW4 computational domain—NIG017, NIG018 and NIG019. To validate the regional attenuation model, free-field surface records are juxtaposed against Ground Motion Prediction Equations (GMPEs) to acknowledge bias in the GMPEs, if any, and then compared with simulated ground motions. In addition to the data available for KKNPP, ground motion records are retrieved from K-NET and KiK-net stations within 40 km of epicentral distance from the database maintained by the National Research Institute for Earth Science and Disaster Resilience<sup>29)</sup> (NIED). Finally, residuals relative to the GMPEs are quantified to contrast between the subsurface models.

## 2. DATA PROCESSING

The data obtained from KKNPP and NIED is filtered following the procedure described by the Pacific Earthquake Engineering Research Center (PEER) for NGA-West2 project<sup>30)</sup> to maintain consistency, for these records are later applied in tandem with the GMPEs from NGA-West2 to evaluate the distance attenuation rate of simulations. Previous work on processing the acceleration data from NIED also proved instrumental in determining the applicable filter bandwidth (Oth et al.<sup>31)</sup>) for these records.

While only the surface sensors are utilized at K-NET and KiK-net to evaluate the accuracy of simulations, both surface and downhole (250 m deep) sensors are employed at SHA to validate site amplification. The orientation of the surface sensors at NIED stations is aligned with the true NS-EW directions but the sensors at KKNPP are aligned with the orientation of the nuclear power plant. Hence, the ground motions from SHA are first rotated to align with the true NS-EW. Azimuths for downhole sensors at SHA are provided by TEPCO and added to the rotation angle accordingly. Once an acceleration history aligned with the true NS-EW directions is obtained, the mean of the record is removed for baseline correction and a cosine taper is applied. Next, the record is padded with zeros and a two-pole two-pass acausal Butterworth filter is applied following Boore et al.<sup>32–34)</sup>. The zero-pads are removed post-filtration and the acceleration history is double integrated to obtain the displacement history. Subsequently, a sixth order polynomial function is fit to the displacement history, and the coefficients for the zeroth and first orders are constrained to 0. Finally, a second derivative of the function is removed from the acceleration history. The processing workflow deviates from the PEER methodology in the last step where instead of reviewing the Fourier spectrum of the displacement, a minimum signal-to-noise ratio (SNR) greater than 3 dB is imposed on the acceleration history using a 15–25 second pre-event noise signal to finalize the filter bandwidths which ensure high quality filtered data (Oth et al.<sup>31)</sup>).

Figure 2 shows the Fourier amplitude spectra of the processed surface motions for both events from SHA and K-NET stations inside the model. Recorded motions at KKNPP contain a lot of long-period noise that is removed by the SNR > 3 dB cutoff for the filter. As a result, the minimum frequency of all spectral comparisons is set by the worst quality record at 0.32 Hz, and the maximum frequency is set at 3 Hz as per the highest frequency resolution of simulations. For response spectra, this roughly translates to 0.33 s – 3 s. From Fig. 2, Event 1 is missing long period energy content and has lower surface amplitudes compared to Event 2, which is consistent with the fact that Event 2 is a larger magnitude event and occurred farther from KKNPP, hence the energy is released into the model over a broader band of frequency.

## 3. REGIONAL SUBSURFACE MODELS

Niigata region is characterized by active geologic folds which have been a subject of various 2D and 3D simulation studies previously (Gatti et al.<sup>35)</sup>, Uetake et al.<sup>36)</sup>, and Hayakawa et al.<sup>37)</sup>). Gatti et al.<sup>35)</sup> summarizes the efforts of several researchers to model the complex folded geologic structure

underneath KKNPP, known as the 3D Ushirodani anticline—Madonosaka syncline—Chuo-Yatai anticline structure, where the models were limited to high shear wave surface velocities because of the computational demands. In this study,  $V_{Smin}$  is set to 130 m/s in site-specific models to accurately represent the site conditions at SHA which, to the authors’ knowledge, is the lowest shear wave velocity ever attempted in regional-scale simulations. The maximum frequency resolution of the simulations is set to 3 Hz to highlight the importance of the low velocity soft layers near the surface. Since  $M_w < 5$  for the simulated events, they are not expected to generate nonlinearity in the soil, maintaining the validity of linear soil behavior assumption in SW4 simulations. The subsurface structure is represented using two different approaches—community velocity model (CVM) and horizontally layered model (HLM). Primitive simulation models consisted of a simple 1D soil profile wherein the vertical propagation of a polarized shear wave was assumed in half-space to evaluate the site response. HLM uses the same 1D profile to populate a 3D space, thereby creating a horizontally layered system, yet is an improvement over the 1D model because it allows 3D wave propagation which facilitates non-vertical incidence, cumulative effect of shear waves, compression waves and surface waves, and inter-wave conversion. The 1D profile can be a representative of average site properties of the model or characterize a specific site of interest, which is KKNPP in this case. HLM is a simplified, homogenous model in lateral extent, which is examined against a community velocity model, an integration of several site and regional investigations, seismic interpretations, and existing 3D models. While CVMs can model the lateral heterogeneity, they generally lack near surface properties and hence cannot replicate site amplifications. The development of CVM and HLM for this study is discussed in the following sections. It is notable that KKNPP lies in a basin, sufficiently far away from any topographical amplifications, hence regional topography is not included in the simulations to keep the models relatively simple. However, the authors acknowledge that topography plays an important role in the scattering of seismic waves and should be addressed in a study focused on a large-scale 3D regional scattering model.

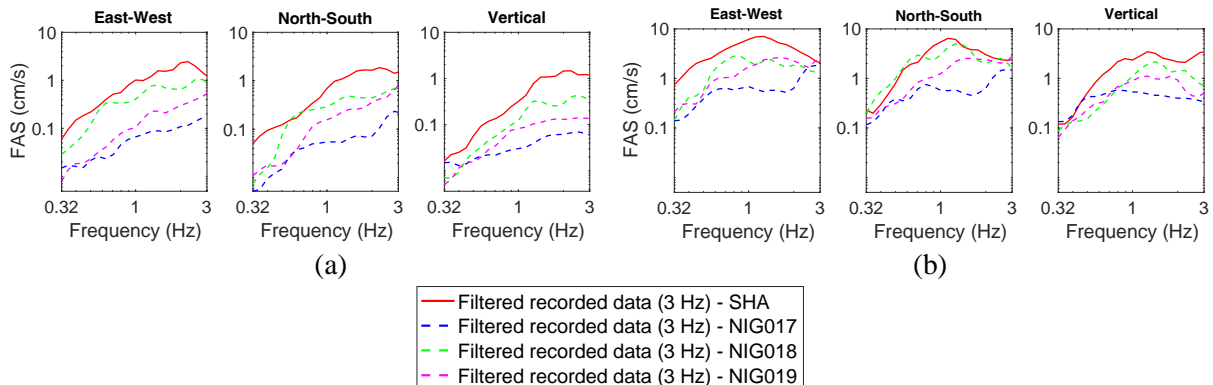


Fig. 2 Fourier amplitudes of three-component surface records from SHA, NIG017, NIG018, and NIG019 for (a) Event 1 and (b) Event 2. The minimum frequency is set by poorest record quality and the maximum by computable frequency of simulations.

### 3.1 Community Velocity Models

The community velocity model is a combination of two different community velocity models available for Japan. The first model comes from the version 2 of the Japan Seismic Hazard Information Station (J-SHIS), used by Fujiwara et al.<sup>38)</sup> for the 2011 version of “Scenario earthquake shaking map” as well as the NGA-West2 project to adjust their models for the regions of Japan. This model has a coarse resolution of 0.9 km and 1.4 km in latitude and longitude respectively and is only 8–10 km deep in the Niigata region. The second model, employed to resolve the geology at greater depths, comes from Japan Integrated Velocity Structure Model (JIVSM). This model is an integration of several datasets from refraction/reflection, microtremor and gravity surveys, borehole loggings and interpretation of seismic records, following a standard procedure proposed by Koketsu et al.<sup>39)</sup>. While

the resolution of JIVSM is the same as that of J-SHIS, it is a deep model created for long-period hazard maps in Japan in 2009 and 2012, and thus is appropriate to fill the remaining depth of the computational model for simulations. Consequently, the J-SHIS model is underlain by the JIVSM to create a 20 km deep CVM. Figures 3(c) and 3(e) illustrate the integrated 2D shear wave velocity profiles across mutually perpendicular planes (A-A' and B-B') with KKNPP at the intersection. The location of the complex geologic fold with respect to KKNPP and the two sources is clearly visible in these figures.

### 3.2 Horizontally Layered Model

To create the horizontally layered model, horizontal sedimentary layers are assumed based on a 1D soil profile. Of the three free-field downhole arrays at KKNPP, SHA is selected because it has reliable ground motion recordings at all seismometers in depth for both the simulated events. The 1D soil profile at SHA is underlain by the 1D profiles extracted from JIVSM and J-SHIS for the coordinates of SHA to create the HLM.

Figure 3(a) presents a unified 1D soil profile obtained from the digitized suspension log for SHA in the upper 120 m (Yee et al.<sup>40</sup>) and a 250 m smoothed soil profile for SHA shared by TEPCO. The final shear wave velocity profiles in depth for HLM are shown in Figs. 3(b) and 3(d), which are contrasted with the depth profiles constructed from the CVM in Figs. 3(c) and 3(e). It is noteworthy that the path between source 2 and KKNPP is planar across section B-B' in Fig. 3(c) and resembles the path in Fig. 3(b) compared to that in section A-A' in Fig. 3(e). Hence, in the absence of any external application of velocity perturbations to the model, the seismic waves are expected to undergo more natural scattering from the geologic fold across section A-A', or in the East-West direction, as opposed to the North-South direction.  $V_{Smin}$  is 130 m/s and 600 m/s for HLM and CVM respectively.

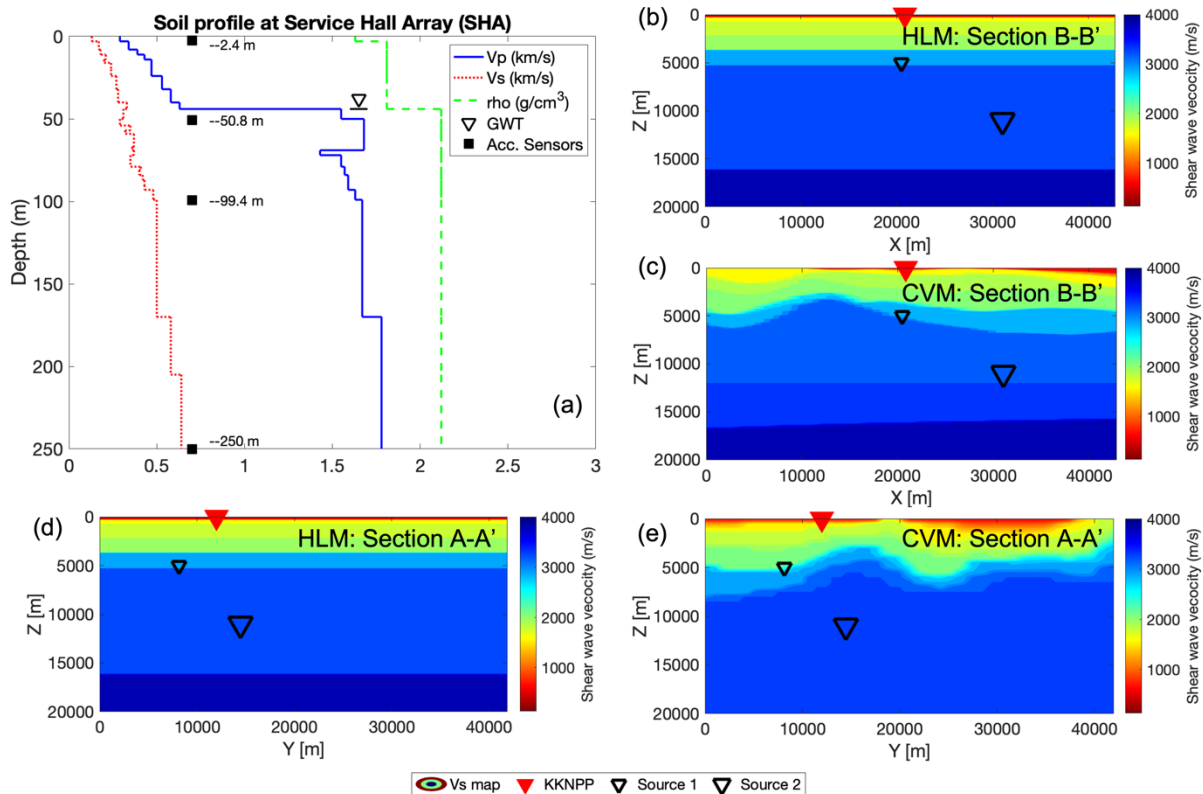


Fig. 3 1D soil profile at SHA used in HLM is shown in (a). 2D depth profiles of shear wave velocity for HLM and CVM across section B-B' from Fig. 1 are shown in (b) and (c) respectively, and across section A-A' are shown in (d) and (e) respectively. In the case of HLM,  $V_{Smin} = 130$  m/s, whereas for CVM,  $V_{Smin} = 600$  m/s.

Since there is no topography in either model, the cut-off elevation is set to the surface elevation of SHA, that is, 67.5 m above Tokyo Mean Sea Level (TMSL). A shallow ground water table (45 m) is present at SHA (Yee et al.<sup>40</sup>) but since there are no current provisions for wave propagation through water in SW4, it is ignored in the simulations.

#### 4. SIMULATION SETUP IN SW4

A large model is setup in SW4, as shown in Fig. 1, to accommodate the seismic sources of the simulated events, KKNPP, and three stations from K-NET—NIG017, NIG018, NIG019. An absorbing boundary of 30 grid points called “supergrid” exists at the boundaries in all directions except the free surface. The absorbing boundary with 2% (default) damping reduces artificial reflections in the model by using a stretching function which mimics a much larger physical domain in each layer. On the other hand, the top or surface boundary in SW4 is traction-free with zero normal stress. Finally, the computational domain extends 42.8 km in x-direction (NS-direction), 41.9 km in y-direction (EW-direction) and 20 km in z-direction (depth).

The maximum frequency resolution of a simulation is dependent on the minimum shear wave velocity in the shallow layers and the smallest applied mesh size. Since the mesh size directly affects the computational resources required to numerically solve the wave propagation throughout the model, the mesh size is optimized to achieve a maximum frequency of 3 Hz. The mesh refinement feature in SW4 facilitates maintenance of 6–10 points per wavelength (PPW) over the varied shear wave velocity profile throughout the depth of the model, following Eq. (1):

$$PPW = \frac{Vs_{min}}{h \times f_{max}} \quad (1)$$

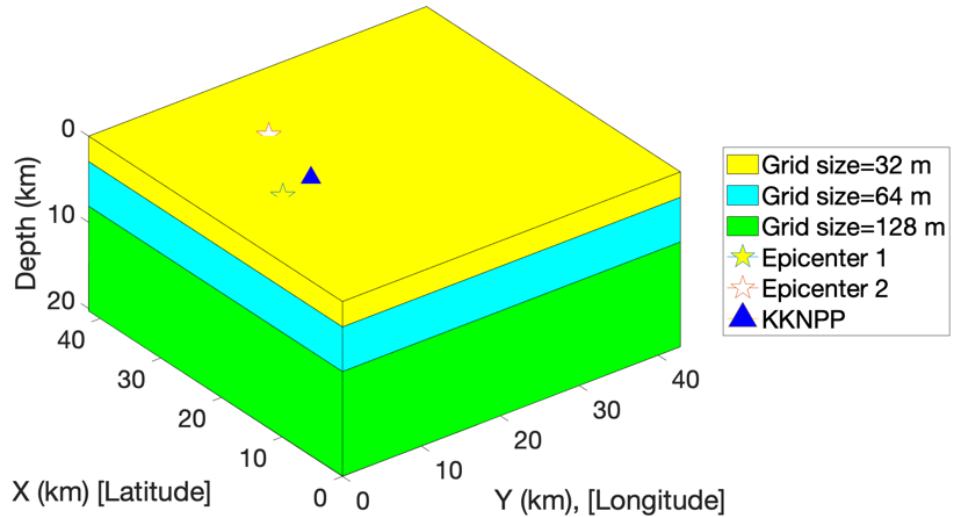
where  $Vs_{min}$  is the minimum shear wave velocity for each grid size,  $h$  is the corresponding size of the grid, and  $f_{max}$  is the maximum frequency resolution desired (3 Hz in this case). Table 2 presents the model specifications as well as the computational demands to run the simulations with CVM and HLM for both events, and Fig. 4 shows the mesh refinement layers in the resulting models. While the largest grid size (128 m) is the same for both models, the smallest grid size at the surface greatly varies due to the large difference in the respective  $Vs_{min}$  applied in the two models. Consequently, up to 25 times the computational resources (CPU-hour) are required for HLM compared to those required for CVM. Only high-performance computing (HPC) can fulfill this kind of computational demand, hence the HPC clusters at Los Alamos National Laboratory (LANL) are utilized for the simulations presented in this research.

Table 2 Model setup and computational demands in SW4

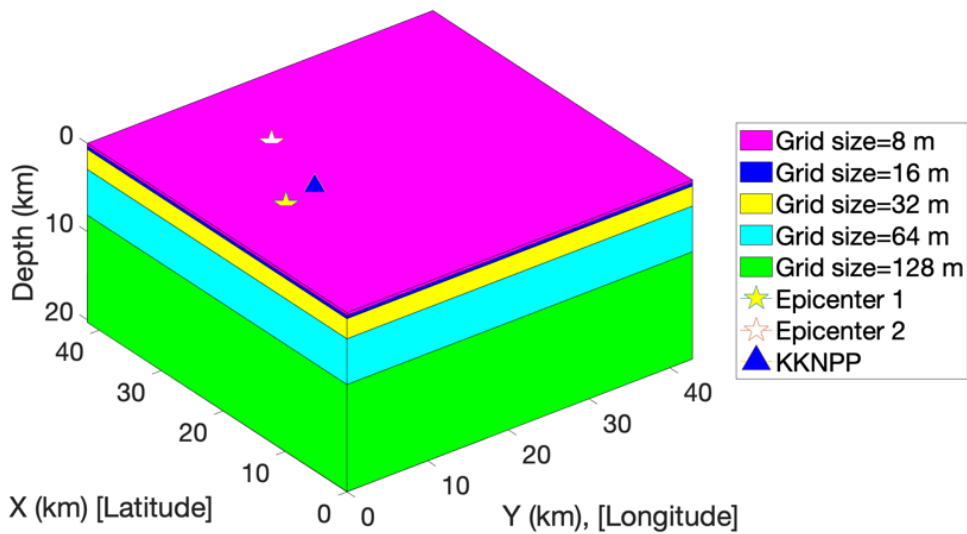
Material Model	$Vs_{min}$ (m/s)	Grid size in the surface layer (m)	Total no. of grid points (million)	Time-step size (s)	CPU-hour (Event 1)	CPU-hour (Event 2)
Community Velocity Model (CVM)	600	32	208	0.00561167	1,008	948
Horizontally Layered Model (HLM)	130	8	856	0.00389469	20,220	24,060

Viscoelastic modeling is enabled in the simulations by superimposing three standard linear solid (SLS) mechanisms, minimum requirement for stable results as per the SW4 User’s Guide<sup>22</sup>, at a reference phase frequency of 1 Hz. Since  $Mw < 5$  for both events, a Gaussian point source is pre-filtered to the maximum computable frequency of the simulation, 3 Hz, to model the seismic source. The filtration is carried out in the SW4 code itself prior to the beginning of the simulation using a

discrete 2<sup>nd</sup> order Butterworth filter with a zero-phase shift. The original Q-model from the CVMs has been used in the HLM as well. Since the Q-model in the CVM was based on a long period range, the authors acknowledge that revising the attenuation model for a high frequency resolution could potentially improve the simulations, though it has not been done in this study.



(a) CVM



(b) HLM

Fig. 4 Mesh refinement implementations for (a) CVM and (b) HLM, based on minimum shear wave velocities near the surface (Table 2)

## 5. RESULTS AND DISCUSSIONS

An overview of the simulation results in the form of peak ground velocity (PGV) magnitude maps for horizontal motions at the surface as observed during the simulation of Event 1 is presented in Fig. 5. Surface amplitudes from the CVM as seen in Fig. 5(a), are much lower than those from the HLM, shown in Fig. 5(b), which is expected due to the lack of near surface properties in the CVM. It is also observed that the classic response to a ‘double couple’ seismic source is visible at the surface from

HLM but not from the CVM. This is due to the lack of wave scattering from lateral homogeneity of geomaterials in the HLM, which also leads to a larger range of influence, however low in magnitude. The next two sub-sections will discuss the performance of the two subsurface models at local/site-specific level as well as regional level.

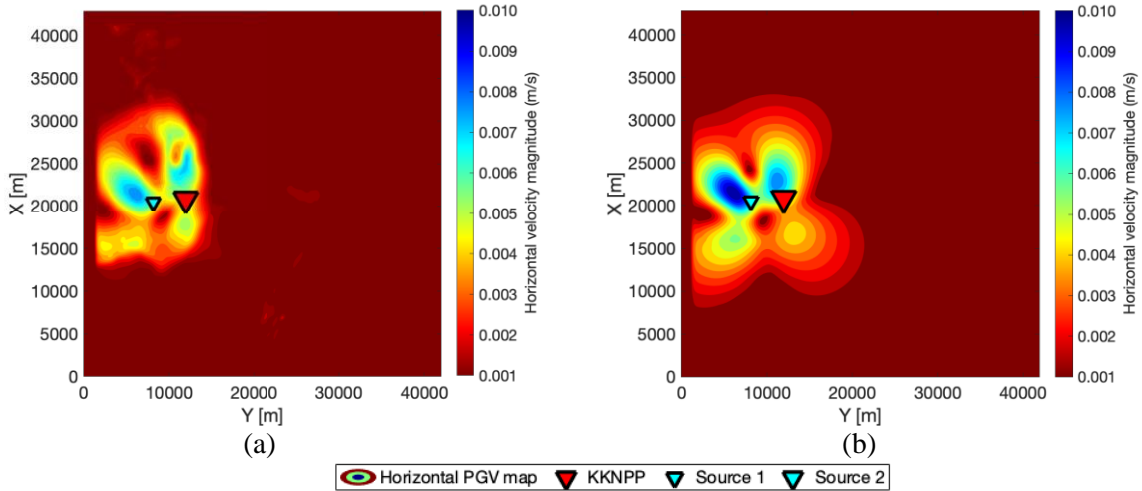


Fig. 5 Horizontal PGV map at the model surface in ‘m/s’ units for (a) CVM and (b) HLM during the simulation of Event 1.

### 5.1 Site-specific comparisons—qualitative and quantitative

Simulated and recorded acceleration histories at the surface and downhole (250 m depth) locations at SHA are compared in Fig. 6 for both events. The first generalized observation made from these results is that while the amplitude of the ground motion is well-captured in most cases, the duration of motion is not. Figures 6(a) and 6(c) show that for Event 1, the peak amplitudes are relatively better at the downhole level, but there is a clear lack of high frequency energy, especially in the P-waves, to be propagated to the surface, indicating the need for a higher frequency source. However, regardless of the low amplitudes for Event 1, it is evident that HLM captures the higher frequency of ground motion better compared to the CVM, thereby highlighting the importance of near surface geotechnical layers. This improvement is better illustrated in the ground motions for Event 2, as seen in Figs. 6(b) and 6(d). In the case of Event 2, the HLM is better at modeling the P-wave and S-wave arrivals and amplitudes in the horizontal as well as the vertical motions compared to the CVM. The source duration for Event 2 (same as that for Event 1) and the source mechanisms from F-net fit the observations well. A common problem in the simulation of both the events is the reconstruction of coda. This problem is expected to resolve with introduction of heterogeneous scattering into the model using velocity perturbations and /or topography. Another significant effect of missing velocity perturbations is seen in the over-estimation of the amplitudes in the NS-component of ground motions for Event 2. Similar over-estimated response was also observed for the previous version of J-SHIS in Fujiwara et al.<sup>41)</sup> and Aochi et al.<sup>42)</sup>. Upon detailed inspection, the over-estimated amplitudes in the NS-component can be seen for both CVM and HLM at the downhole level. However, due to low surface velocities, the over-estimated amplitudes are propagated to the surface only in the case of HLM. It is suggestive of a path effect, not a site effect, that is common to both the models.

Observations parallel to those from time histories are made from the pseudo-spectral acceleration (PSA) plots at the surface and downhole of SHA for Events 1 and 2 in Fig. 7. The improved high frequency content from HLM compared to CVM is evident for both events. The over-estimated response in the NS ground motions for Event 2 can be followed from Fig. 7(b) to the path between source 2 and KKNPP presented in Fig. 3. The cross-section B-B’ in Figs. 3(b) and (c) illustrates a similarity of planar structure between source 2 and KKNPP in the Y-plane which relates to the NS-component of ground motion. Since the wave propagation in these simulations is in 3D and there is

no velocity perturbation in the model, the presence or lack of 3D subsurface structures directly affect the scattering of seismic waves in the CVM. Accordingly, seismic waves from Event 1 and EW-component of Event 2 are sufficiently scattered by the geologic fold, while the energy in the remaining areas is transmitted uninterrupted.

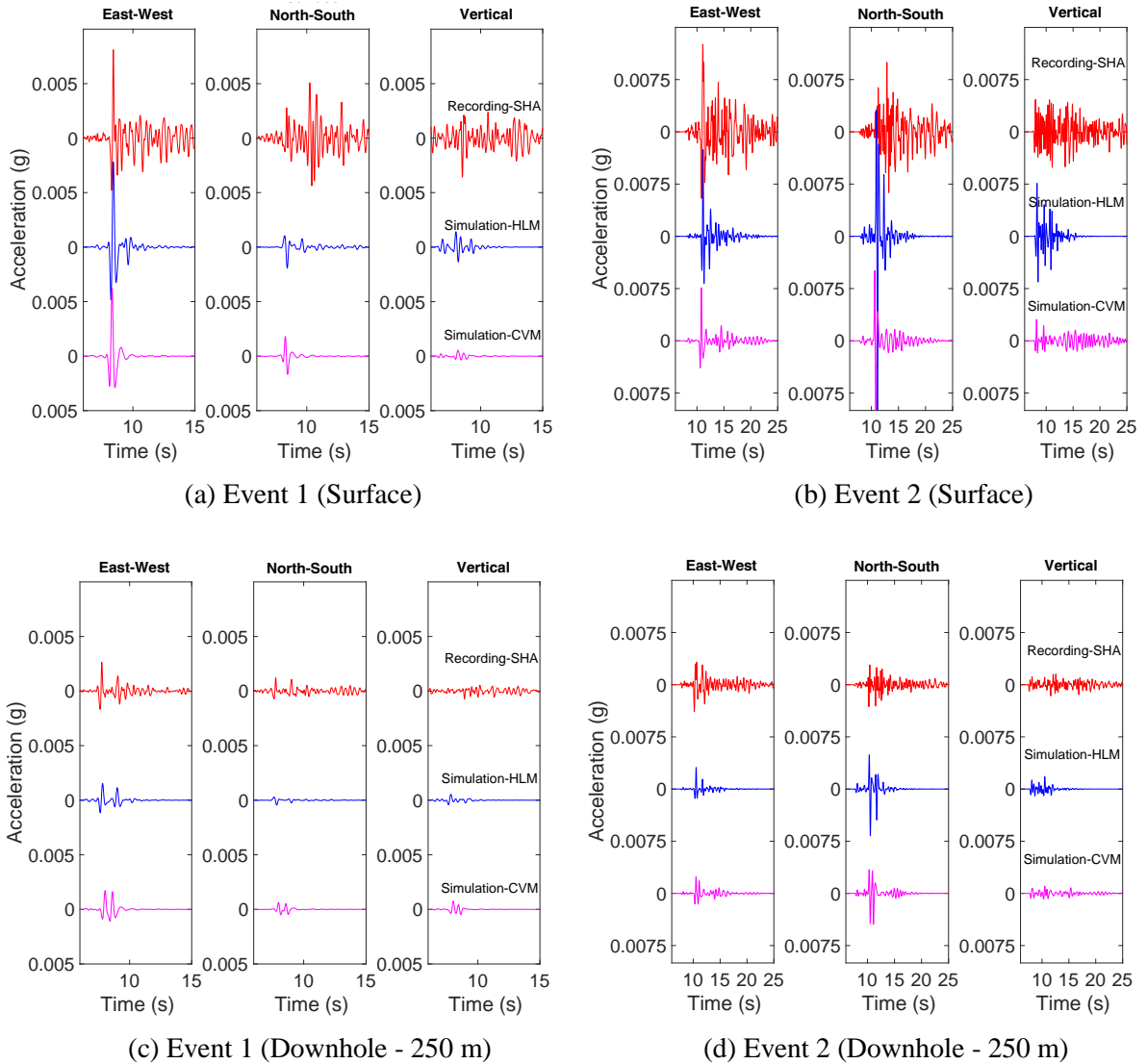


Fig. 6 Acceleration histories at SHA comparing the performance of HLM and CVM with the recorded data for both aftershocks—(a) Event 1 - surface, (b) Event 2 - surface, (c) Event 1 - downhole (250 m), and (d) Event 2 - downhole (250 m). Red is recorded data, blue is HLM simulation, magenta is CVM simulation.

Figure 8 presents amplification factors calculated from the Fourier spectra of surface and downhole (250 m depth) motions at SHA, along with theoretical transfer functions (TTFs) calculated for a layered, damped, 1D soil profile on elastic rock media in half-space (Kramer<sup>43</sup>). The horizontal TTF uses the 1D  $V_s$ -profile whereas the vertical TTF employs the 1D  $V_p$ -profile as employed in the shallow layers (250 m) in HLM. It is noteworthy that the HLM is successful in capturing the dominant modes of site response illustrated by the empirical amplification factors and TTF in the horizontal directions, which are completely missed by the CVM because it lacks the near surface properties, substantiating the importance of geotechnical layers to generate site-specific ground motions. On the other hand, neither the 1D site response demonstrated by the TTF nor the 3D site response from HLM and CVM simulations are able to replicate the surface amplification of vertical ground motion from

aftershock recordings at SHA. A comparison of the horizontal and vertical site response leaves the only possible reason for inaccurate vertical response to be a lack of P-wave interaction with the shallow ground water table present at SHA. A historical context of vertical site response is discussed in detail in section 5.3.

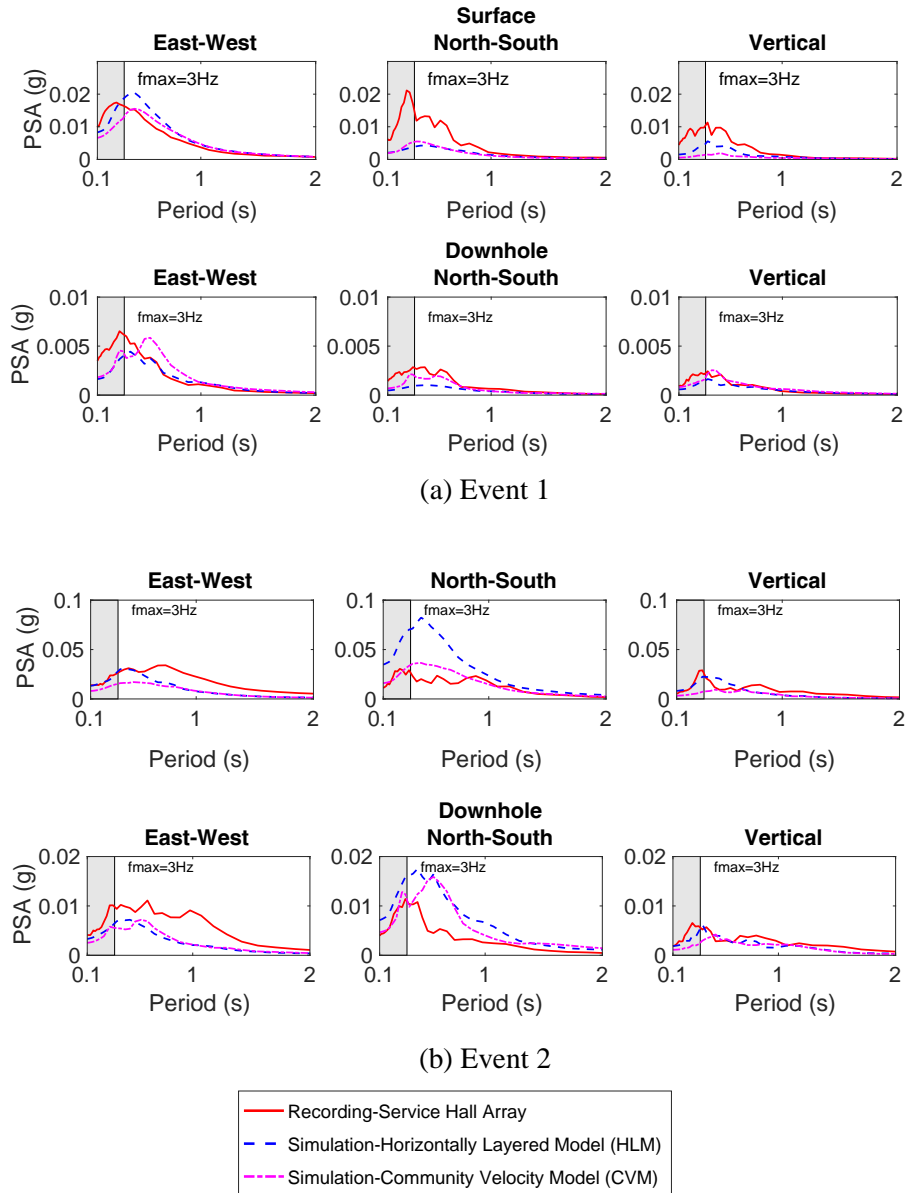


Fig. 7 Maximum SDOF response to recorded and simulated ground motions for (a) Event 1, and (b) Event 2. Minimum resolved period is 0.33 s (corresponding to  $f_{max} = 3$  Hz), as indicated by grey shading.

In addition to the previous qualitative comparisons, a Goodness-of-Fit (GOF) scheme is employed for a rigorous quantitative assessment. The GOF concept was first proposed by Anderson<sup>23)</sup> to quantify the similarity of simulations with the recorded data across ten measurable parameters. Comparing two seismic signals under so many domains gives a comprehensive picture and removes bias. Some of these parameters depend on arrival of the seismic signal and exact waveform comparisons, which are extremely difficult to predict accurately in a large wave propagation model. Hence, a reformed GOF algorithm proposed by Shi and Asimaki<sup>25)</sup> has been adopted to quantify the accuracy (or lack thereof) of the two simulation models. It also provides identification of under-

prediction for  $GOF < 0$ , over-prediction for  $GOF > 0$ , and perfect fit for  $GOF = 0$ . Since Shi and Asimaki<sup>25)</sup> did not provide their own classification system, one was inferred from the original scoring scheme by Anderson<sup>23)</sup> and is presented in Table 3.

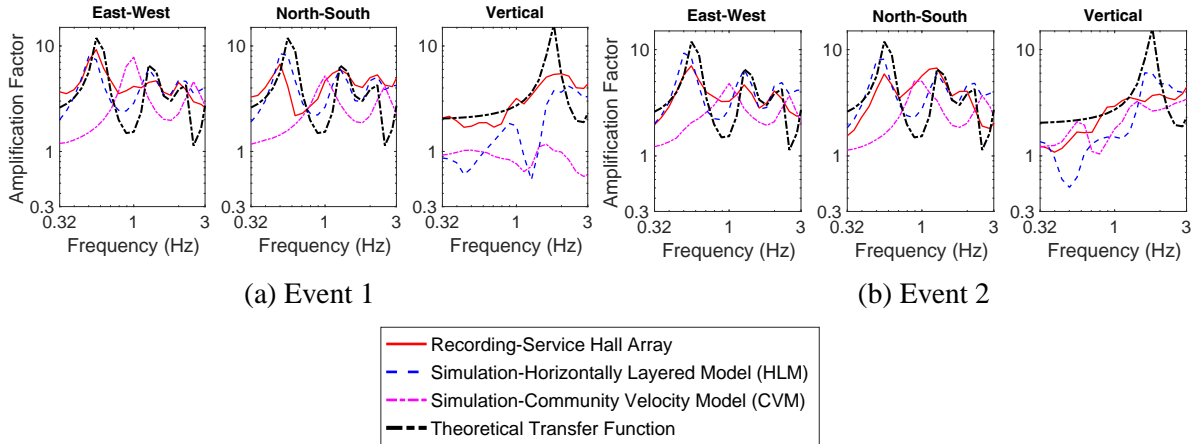


Fig. 8 Amplification factors computed from surface/borehole Fourier spectra for (a) Event 1 and (b) Event 2

Table 3 GOF scoring scheme to classify quality of fit

Range of scores	Quality of fit
0	Perfect
$[-2 \ 0]$ or $[0 \ 2]$	Excellent
$[-2 \ -4]$ or $[2 \ 4]$	Good
$[-4 \ -6]$ or $[4 \ 6]$	Fair
$[-6 \ -10]$ or $[6 \ 10]$	Poor

Figure 9 presents acceleration histories for SHA, NIG017, NIG018, and NIG019 in Figs. 9(a) and (c), beside their GOF scores in Figs. 9(b) and (d). Based on the above scoring scheme, GOF scores for both HLM and CVM are generally in the “good fit” range for both seismic events, with an average absolute score less than 4. At SHA, both the models show an “excellent fit” in the EW direction and a “fair fit” in the NS and vertical directions. It is also detected that HLM generally scores either equivalent or better than CVM at all four stations. This is an important observation because regardless of SHA being the best modeled site, the other three sites also lie in a basin and hence show a general improvement in site response under the influence of low velocity layers of the HLM. An under-prediction of nearly all ground motions for Event 1 is detected from the GOF scores as well.

## 5.2 Regional comparison of SW4 simulations

In this section, a regional assessment of the simulations is carried out against GMPEs from the NGA-West2 project. Four horizontal GMPEs were published in 2014 as an outcome of the NGA-West2 project—Boore et al.<sup>44)</sup> abbreviated as BSSA14, Abrahamson et al.<sup>45)</sup> abbreviated as ASK14, Campbell and Bozorgnia<sup>46)</sup> abbreviated as CB14 and Idriss<sup>47)</sup>. Idriss<sup>47)</sup> does not include small-to-moderate sized earthquakes in its database and is not applicable to sites with time averaged shear-wave velocity in the upper 30 m,  $V_{S30}$ , less than 450 m/s ( $V_{S30}$  at SHA  $\sim 220$  m/s), hence it is not included in the GMPE validations in this study. BSSA14 does not differentiate between mainshock and aftershocks while ASK14 used a separate aftershock scaling based on the Class 1 (mainshock) and Class 2 (aftershock) classification in Wooddell and Abrahamson<sup>48)</sup>. Using the same classification, CB14 did not include aftershocks in its database, yet given its applicability in every other aspect, it is included in the study. Similarly, their vertical counterparts—Stewart et al.<sup>49)</sup>, hereafter SBSA16,

Gulerce et al.<sup>50</sup>, hereafter GKAS17, and Bozorgnia and Campbell<sup>51</sup>, hereafter BC16—are also included to validate the vertical motions separately.

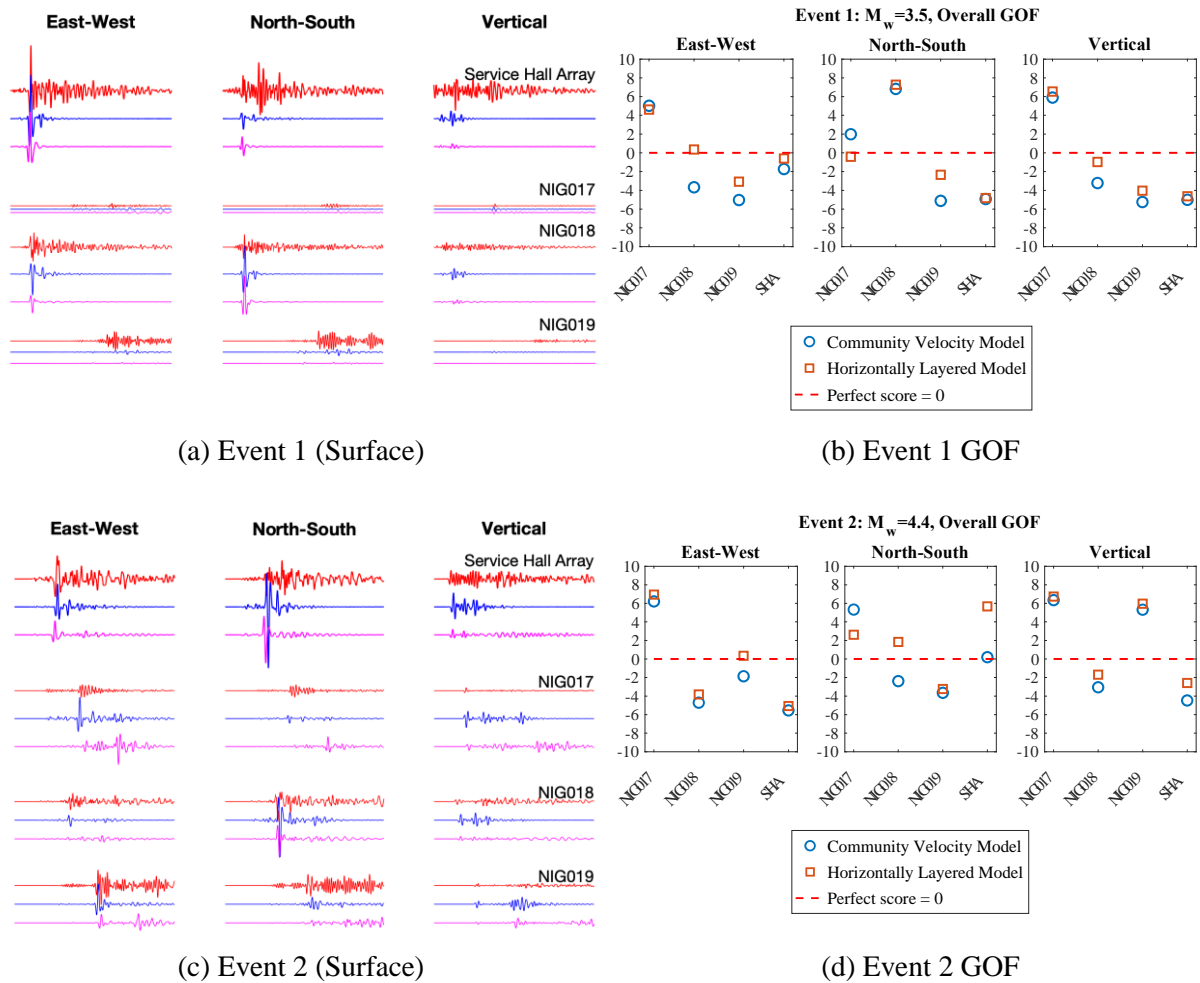


Fig. 9 Recorded and simulated ground motions from SHA, NIG017, NIG018, and NIG019 shown in the left panels and the corresponding GOF scores in the right panels

A dense array consisting of 324 free-field recording stations, placed every 2 km in the NS and EW directions, is defined in SW4 to carry out a regional validation of the two subsurface models. Figure 10 presents the distance attenuation and scattering characteristics of the simulations. Mean, median and standard deviation of natural logarithmic residuals relative to an average of the median predictions from NGA-West2 GMPEs are displayed in each panel. While the mean and median symbolize the accuracy of the attenuation model relative to an average of GMPEs, the standard deviation depicts the magnitude of scattering in the model. These parameters are considered in tandem with any regional bias in the GMPEs, characterized by the PGAs recorded in the region at KKNPP and NIED stations. The records filtered at 25 Hz show that the GMPEs marginally underestimate the PGAs from Event 1 but capture well the median of the PGAs from Event 2. The lowpass filtered records at 3 Hz illustrate that the simulations perform well considering their limited maximum frequency resolution. It must be noted that GKAS17 did not provide median PGA values and hence is absent from vertical PGA comparisons. Average site properties are entered into the GMPEs for distance attenuation plots and site-specific parameters like  $Z_{2.5}$ , depth of soil layer with  $V_s = 2.5$  km/s,  $Z_{1.0}$ , depth of soil layer with  $V_s = 1$  km/s, and  $V_{s30}$  are estimated from different methods for site-specific spectral comparisons.  $Z_{2.5}$  values for each recording station are estimated from the CVM.  $Z_{1.0}$  values were also estimated from the CVM but since the models do not include topography, several  $Z_{1.0}$  values were above the elevation of the model. Hence, a default option for  $Z_{1.0}$  is used in the

GMPEs. Lastly, the values for  $V_{s30}$  are estimated from a kriging algorithm using several 1D soil profiles available in the region. Since only 3 K-NET stations lay inside the computational domain, all the K-NET and KiK-net stations shown in Fig. 1, along with SHA representing KKNPP, were utilized to train a spherical variogram model. Given the lack of data in the area of interest, the kriging resulted in a coarsely interpolated geotechnical layer of 250 m thickness. The authors have used this “Kriging layer” to overlay the CVM to simulate Event 2 in a separate study (Saxena et al.<sup>52</sup>) and concluded that there can be advantages to such a model that combines the advantages of 3D subsurface structures with low velocity near surface layers, but only if the model is well constrained with data.

It can be seen from Figs. 10(a) and 10(c) that for Event 1, CVM estimates are lower than the 3 Hz records, whereas the HLM captures the PGAs well in the horizontal direction and over-estimates them in the vertical. On the other hand, Figs. 10(b) and 10(d) show that for Event 2, the CVM estimates are improved but the HLM are over-estimated. It is evident from the higher values of standard deviation for the CVM simulations and undispersed amplitudes at similar distances observed for the HLM that HLM lacks realistic scattering in propagation of seismic waves, which also leads to very large amplitudes. However, the HLM holds its worth in capturing site-specific response as seen from the amplification factors in Fig. 8. Owing to the location of source 2 (Fig. 3c), the path to most surface stations seems free of complex lateral heterogeneities, explaining the similarity between distance attenuation of the horizontal PGA plots for the CVM and HLM in Fig. 10(b). A qualitative comparison between the median prediction from GMPEs and the recorded data (25 Hz) in Fig. 10 shows a good compatibility, hence the GMPEs are considered suitable for further spectral validations as long the limited 3 Hz frequency output from simulations is also considered in the context.

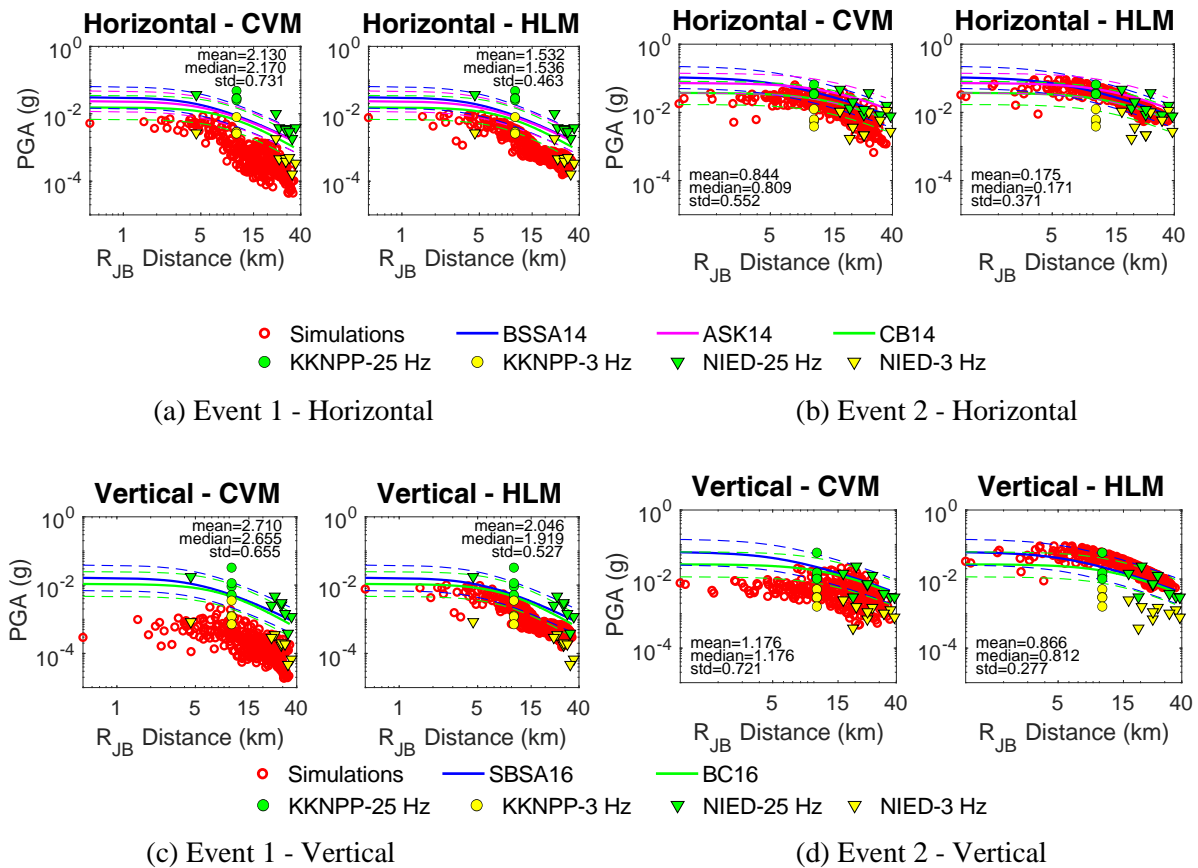


Fig. 10 Distance attenuation plots for PGA for horizontal simulations from CVM and HLM compared with BSSA14, ASK14, and CB14 in (a) Event 1 and (b) Event 2, and vertical simulations compared with SBSA16, and BC16 in (c) Event 1 and (d) Event 2.

To carry out validations at other spectral periods, site-specific parameters are used in the GMPEs to compute pseudo-spectral values (PSA) for vertical motion and orientation-independent PSA, RotD50, for horizontal. Finally, the residuals between GMPEs and simulations are represented by the quantity epsilon, proposed by Rodger et al.<sup>12)</sup>. According to this method, epsilon ( $\varepsilon$ ) is calculated using Eq. (2) as a difference of natural logarithmic intensities of simulations ( $z$ ) and median GMPE predictions ( $\hat{z}$ ), divided by the natural logarithm of standard deviation of the GMPE model,  $\hat{\sigma}$ :

$$\varepsilon = \frac{z - \hat{z}}{\hat{\sigma}} \quad (2)$$

The first advantage of this approach is that it considers expected ground motion variability by directly including standard deviation in the calculation of epsilon. The second advantage is that it can quantify residuals from several GMPEs by assigning an arithmetic mean of the considered GMPEs to  $\hat{z}$  and an average value of standard deviation to  $\hat{\sigma}$ . BSSA14, ASK14, and CB14 are considered for horizontal motions, and SBSA16, GKAS17, and BC16 are considered for vertical motions to calculate epsilon values, which are presented in Fig. 11. Median epsilon values are represented by a thick red line, while standard deviation is shown in yellow for inner 50% range of epsilon (25% – 75%) and blue for inner 90% range of epsilon (5% – 90%). Given the range of standard deviation computed from the GMPEs,  $\pm 1$  epsilon values in these plots usually correspond to 2 or  $\frac{1}{2}$  times of the median PSA respectively. While the horizontal as well as vertical simulations of Event 1 in the left panel of Fig. 11(a) under-predict PSA relative to the GMPEs, horizontal simulations of Event 2 show a good fit with the GMPEs with a median epsilon value of zero for almost the entire applicable range of periods (0.33 s – 3 s). Like the distance attenuation plots, amplitudes for HLM are systematically higher with lower variability compared to the CVM, echoing the importance of a realistic scattering model in 3D simulations. The unrealistically large vertical motions are stemming from limited vertical site response models, as discussed in section 5.3.

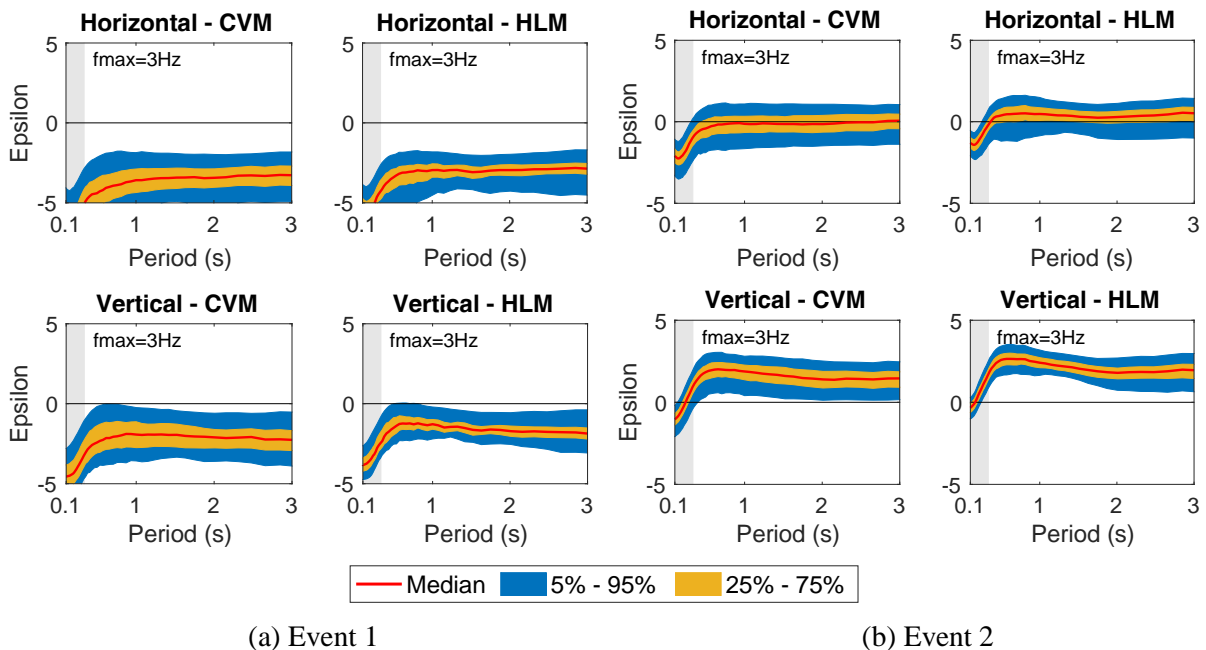


Fig. 11 Epsilon plots comparing CVM and HLM simulations with GMPEs; RotD50 in the upper panels, and vertical PSA in the lower panels. (a) Event 1 and (b) Event 2. Red line indicates the median epsilon surrounded by inner 50% and 90% ranges in yellow and blue shades respectively. Minimum resolved period is 0.33 s (corresponding to  $f_{max} = 3$  Hz)

### 5.3 Additional remarks on regional-scale modeling of vertical motions

Several studies<sup>53)–55)</sup> have confirmed the inadequacy of  $V/H$  ratios to predict vertical ground motions. Bozorgnia et al.<sup>53)</sup> noted that  $V/H$  ratios under-estimate vertical motion at short periods up to 40 km from the source for 1994 Northridge earthquake, which gets significant at shorter distances. Similarly, actual  $V/H$  ratio was observed to be much lower than the prevalent  $V/H = 2/3$  relationship at long periods. Elgamal et al.<sup>54)</sup> reported a similarity in the shape of the vertical response spectra at the surface as well as at downhole while noting that up to 2–3 times surface amplification occurred in just the top 10–20 m. By applying a system identification optimization procedure to a 1D wave propagation model, they determined the dynamic properties of the model, which revealed a very high damping (around 15%) and approximately 75% of the compressional wave ( $V_p$ ) values compared to geophysical measurements. While these studies inspired independent ground motion models for vertical motions (SBSA16, GKAS17, and BC16, for instance), they did not account for P-wave propagation through water. Recalling the shallow ground water table at KKNPP the simulations remain undamped due lack of soil-fluid interaction leading to much higher amplitudes for vertical motions across all relevant periods in Fig. 11 (b). Although Event 1 is generally under-predicted, Fig. 11(a) also shows higher amplitudes for vertical ground motion compared to the horizontal. Tsai and Liu<sup>55)</sup> explain that soil permeability dominates the effect of damping under the propagation of compression wave in a submerged soil layer, and this fluid and P-wave coupling can be modeled by two sets of constrained modulus reduction curves established by the saturation condition of the soil layer. Based on these insights, the authors are considering a finite element modeling exercise using modified modulus reduction curves and damping curves to improve vertical site response.

## 6. CONCLUSIONS

Simulation of seismic ground motions from small-moderate earthquakes is a complex amalgamation of well-tested models for the source, the path, as well as site characteristics. This study examines the advantages and limitations of two regional subsurface models, HLM and CVM, to model the path and site parameters, keeping the source constant. CVM is a community velocity model created from two existing models for Japan which provided a heterogeneous model in 3D but lacked near surface properties. HLM model is generated by propagating a 1D soil profile at SHA in the horizontal directions to form a horizontally layered model. Two aftershocks of the 2007 Niigata-Chuetsu earthquake of 2007 were simulated in a fourth-order accurate finite difference code—SW4. An equally significant parcel of this study is the interpretation of the performance of these models across several key aspects of ground motions, carried out under six different qualitative and/or quantitative validation exercises.

A visual inspection of acceleration histories at SHA shows that the peak ground amplitudes are captured well by both the models for Event 2, however there is scope for improvement in the duration of all ground motion which may be addressed by adjusting the attenuation model, or adding heterogeneous scattering in the models through topography and/or velocity perturbations. The NS-component of ground motion is over-estimated at the downhole by both the models for Event 2, which is also an effect of lack of velocity perturbations. The response spectral plots reveal that HLM is more effective in capturing the high frequency site response in the horizontal as well as vertical directions at SHA. Amplification plots also highlight the success of HLM in reproducing site amplification in the horizontal direction, though the vertical site response was not reconstructed as well. Since the SW4 computational model represents a shallow basin, the HLM mostly out-performs the CVM, as concluded from the GOF scores.

For regional comparisons, GMPEs from NGA-West2 are plotted in conjunction with recorded ground motions from all the free-field stations at KKNPP, as well as nearby K-NET and KiK-net stations. Standard deviation of the residuals between simulations and GMPEs are quantified, which show lower value for HLM compared to CVM, revealing a lack of 3D scattering model. Epsilon plots

are employed to quantify the median and variability of residuals across the applicable period range. They show a very good comparison for the horizontal motions of Event 2 but highly over-estimated vertical motions, thus underlining the significance of modified vertical site response models, which are also discussed.

In conclusion, HLM performs either similar to or better than CVM in capturing high frequency site response. However, it consistently over-predicts the surface amplitudes due to lack of a scattering model. This work inspired another investigation into an ideal model that would combine the advantages of a CVM with low velocity geotechnical layers. The results of that study indicate a limited improvement until more data is available to constrain the model. All the validation schemes suggest that Event 1 is generally under-estimated, necessitating a deeper look into the source duration, which was neglected in this study. The authors have noted potential enhancements in the simulations using a higher frequency source model for Event 1 which will advance future research that will simultaneously look into improving vertical site response analysis in a finite element soil-structure-interaction model of one of the reactor buildings at KKNPP. These development areas are highlighted by different validation exercises, which is the value of a strong validation scheme.

## ACKNOWLEDGMENT

This work is funded by the Nuclear Safety Research and Development (NSR&D) Program, which is managed by the Office of Nuclear Safety within the Office of Environment, Health, Safety, and Security (AU) to provide corporate-level leadership supporting nuclear safety research and development throughout the Department of Energy (DOE). The authors would like to thank Patrick Frias from the NSR&D Program for the sponsorship of this study. The authors also acknowledge that the ground motion data from KKNPP used in this study belong to Tokyo Electric Power Company and Chubu Electric Power Company, and the distribution license of the data belongs to the Japan Association for Earthquake Engineering. Michael Salmon and Richard Lee, our collaborators at Los Alamos National Laboratory (LANL), were an invaluable support during this work, and Carene Larmat generously provided access to LANL's institutional high-performance computing resources. Special acknowledgement to John Louie, Michelle (Dunn) Scalise, and Eric Eckert in the Department of Geological Sciences and Engineering at the University of Nevada Reno, and Arthur Rodgers from Lawrence Livermore National Laboratory (LLNL), for their insights into regional-scale seismic simulations and SW4.

## REFERENCES

- 1) Boore, D. M.: Finite Difference Methods for Seismic Wave Propagation in Heterogeneous Materials, *Methods in Computational Physics*, Vol. 11, Seismology: Surface waves and Earth oscillations, Academic Press, pp. 1–37, 1972.
- 2) Hartzell, S.: Earthquake Aftershocks as Green's Functions, *Geophysics Research Letters*, Vol. 5, pp. 1–4. <https://doi.org/10.1029/GL005i001p00001>
- 3) Olsen, K. B., Archuleta, R. J. and Matarrese, J. R.: Three-Dimensional Simulation of a Magnitude 7.75 Earthquake on the San Andreas Fault, *Science*, Vol. 270, No. 5242, pp. 1628–1632, 1995.
- 4) Graves, R. W.: Simulating Seismic Wave Propagation in 3D Elastic Media Using Staggered-Grid Finite Differences, *Bulletin of Seismological Society of America*, Vol. 86, No. 4, pp. 1091–1106, 1996.
- 5) Pitarka, A.: 3D Elastic Finite Difference Modeling of Seismic Wave Propagation Using Staggered Grid with Non-Uniform Spacing, *Bulletin of Seismological Society of America*, Vol. 88, pp. 54–68, 1999.
- 6) Sjögreen, B. and Petersson, N. A.: A Fourth Order Accurate Finite Difference Scheme for the Elastic Wave Equation in Second Order Formulation, *Journal of Scientific Computing*, Vol. 52, No. 1, pp. 17–48, 2012. <https://doi.org/10.1007/s10915-011-9531-1>

- 7) Bao, H., Bielak, J., Ghattas, O., Kallivokas, L. F., O'Hallaron, D. R., Shewchuk, J. R. and Xu, J.: Large-Scale Simulation of Elastic Wave Propagation in Heterogeneous Media on Parallel Computers, *Computer Methods in Applied Mechanics and Engineering*, Vol. 152, pp. 85–102, 1998.
- 8) Gatti, F., Touhami, S., Lopez-Caballero, F., Paolucci, R., Clouteau, D., Fernandes, V. A., Kham, M. and Voldoire, F.: Broad-Band 3-D Earthquake Simulation at Nuclear Site by an All-Embracing Source-to-Structure Approach, *Soil Dynamics and Earthquake Engineering*, Vol. 115, pp. 263–280, 2018. <https://doi.org/10.1016/j.soildyn.2018.08.028>
- 9) Peter, D., Komatitsch, D., Luo, Y., Martin, R., Le Goff, N., Casarotti, E., Le Loher, P. et al.: Forward and Adjoint Simulations of Seismic Wave Propagation on Fully Unstructured Hexahedral Meshes, *Geophysical Journal International*, Vol. 186, No. 2, pp. 721–739, 2011. <https://doi.org/10.1111/j.1365-246X.2011.05044.x>
- 10) Afanasiev, M., Boehm, C., Driel, M. V., Krischer, L., Rietmann, M., May, D. A., Knepley, M. G. and Fichtner, A.: Modular and Flexible Spectral-Element Waveform Modelling in Two and Three Dimensions, *Geophysical Journal International*, Vol. 216, No. 3, pp. 1675–1692, 2018. <https://doi.org/10.1093/gji/ggy469>
- 11) Anderson, J. G. and Brune, J. N.: Probabilistic Seismic Hazard Analysis without the Ergodic Assumption, *Seismological Research Letters*, Vol. 70, No. 1, pp. 19–28, 1999. <https://doi.org.unr.idm.oclc.org/10.1785/gssrl.70.1.19>
- 12) Rodgers, A. J., Pitarka, A., Pankajakshan, R., Sjögreen, B. and Petersson, N. A.: Regional-Scale 3D Ground-Motion Simulations of Mw 7 Earthquakes on the Hayward Fault, Northern California Resolving Frequencies 0–10 Hz and Including Site-Response Corrections, *Bulletin of Seismological Society of America*, Vol. 110, No. 6, pp. 2862–2881, 2020. <https://doi.org/10.1785/0120200147>
- 13) McCallen, D., Tang, H., Wu, S., Eckert, E., Huang, J. and Petersson, N. A.: Coupling of Regional Geophysics and Local Soil-Structure Models in the EQSIM Fault-to-Structure Earthquake Simulation Framework, *The International Journal of High Performance Computing Applications*, Vol. 36, No. 1, 2022. <https://doi.org/10.1177/10943420211019118>
- 14) McCallen, D., Petersson, N. A., Rodgers, A., Pitarka, A., Miah, M., Petrone, F., Sjögreen, B., Abrahamson, N. and Tang, H.: EQSIM—A Multidisciplinary Framework for Fault-to-Structure Earthquake Simulations on Exascale Computers Part 1: Computational Models and Workflow, *Earthquake Spectra*, Vol. 37, No. 2, pp. 707–735, 2021. <https://doi.org/10.1177/8755293020970982>
- 15) Taborada, R. and Bielak, J.: Ground-Motion Simulation and Validation of the 2008 Chino Hills, California, Earthquake, *Bulletin of Seismological Society of America*, Vol. 103, No. 1, pp. 131–156, 2013. <https://doi.org/10.1785/0120110325>.
- 16) Petersson, N. A. and Sjögreen, B.: geodynamics/sw4: SW4, version 2.01 (Version v2.01). Zenodo, 2017. <http://doi.org/10.5281/zenodo.1063644>
- 17) Kayen, R., Collins, B. D., Abrahamson, N. A., Ashford, S., Brandenberg, S. J., Cluff, L., Dickenson, S. et al.: Investigation of the M6.6 Niigata-Chuetsu Oki, Japan, Earthquake of July 16, 2007, *U.S. Geological Survey, Open File Report 2007–1365*. <http://pubs.usgs.gov/of/2007/1365/>
- 18) Pavlenko, O. V. and Irikura, K.: Nonlinear Soil Behaviour at the Kashiwazaki-Kariwa Nuclear Power Plant During the Niigata Chuetsu-Oki Earthquake (July, 16, 2007), *Pure and Applied Geophysics*, Vol. 169, pp. 1777–1800, 2012.
- 19) Uetake, T., Hikima, K., Sekine, S. and Sawada, Y.: Spatial Variability of Ground Motion of Niigata-Ken Chuetsu Area During the 2011 off the Pacific Coast of Tohoku Earthquake—Analysis of the Data from Dense Observation Array, *Journal of Japan Association for Earthquake Engineering*, Vol. 16, No. 4, pp. 66–79, 2016. [https://doi.org/10.5610/jaee.16.4\\_66](https://doi.org/10.5610/jaee.16.4_66)
- 20) Saxena, S., Motamed, R. and Ryan, K.: Effects of Subsurface Soil Spatial Variability on Recorded Ground Motions at Kashiwazaki-Kariwa Nuclear Power Plant. *Proceedings of Structural Mechanics in Reactor Technology (SMiRT 25)*, Charlotte, NC, pp. 1469–1478, 2019.

- 21) Kubo, A., Fukuyama, E., Kawai, H. and Nonomura, K.: NIED Seismic Moment Tensor Catalogue for Regional Earthquakes Around Japan: Quality Test and Application, *Tectonophysics*, Vol. 356 No. 1, pp. 23–48, 2002. [http://doi.org/10.1016/S0040-1951\(02\)00375-X](http://doi.org/10.1016/S0040-1951(02)00375-X)
- 22) Petersson, N. A. and Sjogreen, B.: SW4 User's Guide v.2.0, 2017. <https://geodynamics.org/cig/software/github/sw4/v2.01/SW4-UsersGuide.pdf> (last accessed on August 1, 2022)
- 23) Anderson, J. G.: Quantitative Measure of the Goodness-of-Fit of Synthetic Seismograms, *Proceedings of 13th World Conf. on Earthquake Engineering*, Vancouver, British Columbia, International Association of Earthquake Engineering, 2004.
- 24) Olsen, K. B. and Mayhew, J. E.: Goodness-of-Fit Criteria for Broadband Synthetic Seismograms, with Application to the 2008 Mw 5.4 Chino Hills, California, Earthquake, *Seismological Research Letters*, Vol. 81, No. 5, pp. 715–723, 2010. <http://doi.org/10.1785/gssrl.81.5.715>
- 25) Shi, J. and Asimaki, D.: From Stiffness to Strength: Formulation and Validation of a Hybrid Hyperbolic Nonlinear Soil Model for Site-Response Analyses. *Bulletin of Seismological Society of America*, Vol. 107, No. 3, pp. 1336–1355, 2017. <http://doi.org/10.1785/0120150287>
- 26) Rodgers, A. J., Petersson, N. A., Pitarka, A., McCallen, D. B., Sjogreen, B. and Abrahamson, N.: Broadband (0–5 Hz) Fully Deterministic 3D Ground-Motion Simulations of a Magnitude 7.0 Hayward Fault Earthquake: Comparison with Empirical Ground Motion Models and 3D Path and Site Effects from Source Normalized Intensities, *Seismological Research Letters*, Vol. 90, No. 3, pp. 1268–1284, 2019. <http://doi.org/10.1785/0220180261>
- 27) Lee, R. L., Bradley, B. A., Stafford, O. J., Graves, R. W. and Rodriguez-Marek, A.: Hybrid Broadband Ground Motion Simulation Validation of Small Magnitude Earthquakes in Canterbury, New Zealand, *Earthquake Spectra*, Vol. 36, No. 2, pp. 673–699, 2020. <http://doi.org/10.1177/8755293019891718>
- 28) Petrone, F., Abrahamson, N., McCallen, D. and Miah, M.: Validation of (Non-Historical) Large-Event Near-Fault Ground-Motion Simulations for Use in Civil Engineering Applications, *Earthquake Engineering Structural Dynamics*, Vol. 50, pp. 116–134, 2020. <http://doi.org/10.1002/eqe.3366>
- 29) National Research Institute for Earth Science and Disaster Resilience, NIED K-NET, KiK-net, *National Research Institute for Earth Science and Disaster Resilience*, 2019. doi: 10.17598/NIED.0004
- 30) Bozorgnia, Y., Abrahamson, N. A., Atik, L. A., Ancheta, T. D., Atkinson, G. M., Baker, J. W., Baltay, A. et al.: NGA-West2 Research Project, *Earthquake Spectra*, Vol. 30, No. 3, pp. 973–987, 2014. <http://doi.org/10.1193/072113EQS209M>
- 31) Oth, A., Parolai, S. and Bindi, D.: Spectral Analysis of K-NET and KiK-net Data in Japan, Part I: Database Compilation and Peculiarities. *Bulletin of Seismological Society of America*, Vol. 101, No. 2, pp. 652–666, 2011. <http://doi.org/10.1785/0120100134>
- 32) Boore, D. M. and Akkar, S.: Effect of Causal and Acausal Filters on Elastic and Inelastic Response Spectra, *Earthquake Engineering Structural Dynamics*, Vol. 32, pp. 1729–1748, 2003. <http://doi.org/10.1002/eqe.299>
- 33) Boore, D. M. and Bommer, J. J.: Processing of Strong-Motion Accelerograms: Needs, Options and Consequences, *Soil Dynamics and Earthquake Engineering*, Vol. 25, pp. 93–115, 2005.
- 34) Boore, D. M., Sisi, A. A. and Akkar, S.: Using Pad-Stripped Acausally Filtered Strong-Motion Data, *Bulletin of Seismological Society of America*, Vol. 86, No. 2, pp. 751–760, 2012. <http://doi.org/10.1785/0120110222>
- 35) Gatti, F., Lopez-Caballero, F., Clouteau, D. and Paolucci, R.: On the Effect of the 3-D Regional Geology on the Seismic Design of Critical Structures: The Case of the Kashiwazaki-Kariwa Nuclear Power Plant, *Geophysical Journal International*, Vol. 213, No. 2, pp. 1073–1092, 2018. <http://doi.org/10.1093/gji/ggy027>
- 36) Uetake, T., Tokumitsu, R., Nishimura, I. and Hijikata, K.: Effects of Fold Structure in the Kashiwazaki-Kariwa Nuclear Power Station on the Ground Motion Characteristics of Niigataken Chuetsu-Oki Earthquake—Modeling of Sub-Surface Structure and Wave Propagation Study

- Using a Finite Difference Method, *Journal of Structural and Construction Engineering (Transactions of AIJ)*, Vol. 76, No. 660, pp. 311–318, 2011. <https://doi.org/10.3130/aijs.76.311>
- 37) Hayakawa, T., Shimmura, A., Hikima, K. and Uetake, T.: Modeling a 3-D Velocity Structure Around the Kashiwazaki-Kariwa Nuclear Power Plant for Evaluation of Long Period Strong Ground Motions, *Journal of Japan Association for. Earthquake Engineering*, Vol. 20, No. 3, pp. 1–20, 2020. [https://doi.org/10.5610/jaee.20.3\\_1](https://doi.org/10.5610/jaee.20.3_1)
  - 38) Fujiwara, H., Kawai, S., Aoi, S., Morikawa, N., Senna, S., Azuma, H., Ooi, M. et al.: Some Improvements of Seismic Hazard Assessment based on the 2011 Tohoku Earthquake, *Technical Note of the National Research Institute for Earth Science and Disaster Prevention*, No. 379, 2012 (in Japanese).
  - 39) Koketsu, K., Miyake, H. and Suzuki, H.: Japan Integrated Structure Velocity Model version 1, *Proceedings of 13th World Conference on Earthquake Engineering*, Lisbon, Portugal, International Association of Earthquake Engineering, 2012.
  - 40) Yee, E., Stewart, J. P. and Tokimatsu, K.: Elastic and Large-Strain Nonlinear Seismic Site Response from Analysis of Vertical Array Recordings, *Journal of Geotechnical and Geoenvironmental Engineering, ASCE*, Vol. 139, No. 10, pp. 1789–1801, 2013. [https://doi.org/10.1061/\(ASCE\)GT.1943-5606.0000900](https://doi.org/10.1061/(ASCE)GT.1943-5606.0000900)
  - 41) Fujiwara, H., Kawai, S., Aoi, S., Morikawa, N., Senna, S., Kudo, N., Ooi, M. et al.: A Study on Subsurface Structure Model for Deep Sedimentary Layers of Japan for Strong-Motion Evaluation, *Technical Note of the National Research Institute for Earth Science and Disaster Prevention*, No. 337, 2009 (in Japanese).
  - 42) Aochi, H., Ducellier, A., Dupros, F., Delatre, M., Ulrich, T., Martin, F. and Yoshimi, M.: Finite Difference Simulations of Seismic Wave Propagation for the 2007 Mw 6.6 Niigata-ken Chuetsu-Oki Earthquake: Validity of Models and Reliable Input Ground Motion in the Near-Field. *Pure and Applied Geophysics*, Vol. 170, pp. 43–64, 2013. <https://doi.org/10.1007/s00024-011-0429-5>
  - 43) Kramer, S. L.: Chapter 7 Ground Response Analysis, *Geotechnical Earthquake Engineering*, 1st ed., Prentice Hall, pp. 254–303, 1996.
  - 44) Boore, D. M., Stewart, J. P., Seyhan, E. and Atkinson, G. M.: NGA-West2 Equations for Predicting PGA, PGV, and 5% Damped PSA for Shallow Crustal Earthquakes, *Earthquake Spectra*, Vol. 30, No. 3, pp. 1057–1085, 2014. <https://doi.org/10.1193/070113EQS184M>
  - 45) Abrahamson, N. A., Silva, W. J. and Kamai, R.: Summary of the ASK14 Ground Motion Relation for Active Crustal Regions, *Earthquake Spectra*, Vol. 30, No. 3, pp. 1025–1055, 2014. <https://doi.org/10.1193/070913EQS198M>
  - 46) Campbell, K. W. and Bozorgnia, Y.: NGA-West2 Ground Motion Model for the Average Horizontal Components of PGA, PGV, and 5% Damped Linear Acceleration Response Spectra, *Earthquake Spectra*, Vol. 30, No. 3, pp. 1087–1115, 2014. <https://doi.org/10.1193/062913EQS175M>
  - 47) Idriss, I. M.: An NGA-West2 Empirical Model for Estimating the Horizontal Spectral Values Generated by Shallow Crustal Earthquakes, *Earthquake Spectra*, Vol. 30, No. 3, pp. 1155–1177, 2014. <https://doi.org/10.1193/070613EQS195M>
  - 48) Wooddell, K. E. and Abrahamson, N. A.: Classification of Main Shocks and Aftershocks in the NGA-West2 Database, *Earthquake Spectra*, Vol. 30, No. 3, pp. 1257–1267, 2014. <https://doi.org/10.1193/071913EQS208M>
  - 49) Stewart, J. P., Boore, D. M., Seyhan, E. and Atkinson, G. M.: NGA-West2 Equations for Predicting Vertical-Component PGA, PGV, and 5%-Damped PSA from Shallow Crustal Earthquakes, *Earthquake Spectra*, Vol. 32, No. 2, pp. 1005–1031, 2016. <https://doi.org/10.1193/072114eqs116m>
  - 50) Gülerce, Z., Kamai, R., Abrahamson, N. A. and Silva, W. J.: Ground Motion Prediction Equations for the Vertical Ground Motion Component Based on the NGA-WEST2 Database, *Earthquake Spectra*, Vol. 33, No. 2, pp. 499–528, 2017. <https://doi.org/10.1193/121814EQS213M>

- 51) Bozorgnia, Y. and Campbell, K. W.: Vertical Ground Motion Model for PGA, PGV, and Linear Response Spectra Using the NGA-West2 Database, *Earthquake Spectra*, Vol. 32, No. 2, pp. 979–1004, 2016. <https://doi.org/10.1193/072814eqs121m>
- 52) Saxena, S., Motamed, R. and Ryan, K. L.: Large-Scale 3D Ground Motion Simulations of a Moderate-Sized Earthquake at Kashiwazaki-Kariwa Nuclear Power Plant in Japan, *Geo-Congress 2022: Geophysics in Geotechnical Practice: 2022*, Charlotte, NC, pp. 92–101, 2021. <https://doi.org/10.1061/9780784484043.009>
- 53) Bozorgnia, Y., Niazi, M. and Campbell, K.W.: Characteristics of Free-Field Vertical Ground Motion During the Northridge Earthquake, *Earthquake Spectra*, Vol. 11, No. 4, pp. 515–525, 1995. <https://doi.org/10.1193/1.1585825>
- 54) Elgamal, A. and He, L.: Vertical Earthquake Ground Motion Records: An Overview, *Journal of Earthquake Engineering*, Vol. 8, No. 5, pp. 663–697, 2004. <https://doi.org/10.1080/13632460409350505>
- 55) Tsai, C.-C. and Liu, H.-W.: Site Response Analysis of Vertical Ground Motion in Consideration of Soil Nonlinearity, *Soil Dynamics and Earthquake Engineering*, Vol. 102, pp. 124–136, 2017. <https://doi.org/10.1016/j.soildyn.2017.08.024>

(Submitted: November 21, 2021)  
(Accepted: August 24, 2022)